AEROTHERMAL DATABASES AND CFD BASED LOAD PREDICTIONS

*M. Laureti *, S. Karl *, A. Marwege ** and A. Gülhan ***

* DLR Institute of Aerodynamics and Flow Technology
Bunsenstr. 10, 37073 Göttingen, Germany
mariasole.laureti@dlr.de - sebastian.karl@dlr.de

** DLR Institute of Aerodynamics and Flow Technology,
Supersonic and Hypersonic Technologies Department
Linder Höhe, 51147 Cologne, Germany
ansgar.marwege@dlr.de - ali.guelhan@dlr.de

ABSTRACT

The RETALT (Retro Propulsion Assisted Landing Technologies) project aims at investigating launch system reusability technologies for two different Vertical Take-off Vertical Landing launcher configurations, namely RETALT1 and RETALT2. This paper describes and summarizes the CFD based aerothermal load predictions, aerothermal database generation and application for the RETALT1 configuration for the complete trajectory. Furthermore, an analysis of representative CFD (Computational Fluid dynamic) results is provided with the aim to show typical flow field phenomena and the resulting heating patterns occurring during the retro-propulsion phase. CFD results are then validated by comparison with the wind tunnel experiments carried out at different ground testing facilities in DLR Cologne.

Index Terms— Reusable Launch Vehicle, Retro-Propulsion, Aerothermal Loads, Wind Tunnel Experiments, CFD, RANS

1. INTRODUCTION

The Retro Propulsion Assisted Landing Technologies (RETALT) project, funded by the European Union Horizon 2020 program (grant agreement No 821890), has as objective to study critical technologies for Vertical Takeoff Vertical Landing (VTVL) Reusable Launch Vehicles (RLVs) applying retro propulsion combined with Aerodynamic Control Surfaces (ACS) [1]. Two reference launch vehicle configurations are defined:

- RETALT1: A heavy lift Two Stage To Orbit (TSTO) RLV with a payload of up to 14 t into the Geo Transfer Orbit (GTO). The first stage, the only one to be recovered, is powered by nine LOX/LH2 engines inspired to the Ariane' s Vulcain 2. The general layout of the RETALT1 configuration is similar to the SpaceX rocket "Falcon 9".
- RETALT2 A smaller Single Stage To Orbit (SSTO) configuration which is capable to deliver 500kg into Low Earth Orbits (LEO) similar to DC-X. The recovery of the full vehicle is foreseen.

The layout and system analysis of reusable launch vehicles include major challenges related to the application of a robust, light-weight, inexpensive and serviceable Thermal Protection System (TPS) [2]. The correct sizing of such a system, as well as other important structural parts like the aerodynamic control surfaces [3, 4, 5] and landing legs [6], relies on an accurate evaluation of thermal loads occurring during the entire atmospheric flight path [7].

The assessment of thermal loads, occurring on reusable launch vehicles during the entire trajectory, relies mainly on numerical simulations (CFD) due to the extremely high costs and limitations associated to extensive experimental campaigns on large-scale vehicles.

This paper describes the structure and construction of a surrogate aero-thermodynamic model, called Aero-Thermal Data Base (ATDB), which consists of a set of steady-state CFD results for the surface heat fluxes at different trajectory points, operational conditions of the engines and surface temperatures. The aero-thermal database created for the RETALT1 vehicle is based on a computational matrix that covers the entire flight trajectory in particular the flight regimes characterised by significant thermal loads or high dynamic pressure. In order to evaluate the heat flux on each point of the rocket surface as function of flight time and local surface temperature, interpolation algorithms are implemented. Finally the ATDB can be easily coupled to a structural response model to estimate the temperature history in each location on the vehicle surface during the entire trajectory.

The aim of this paper is also to analyse the results of representative CFD simulations, carried out for the aero-thermal data base construction, highlighting the presence of typical flow field phenomena occurring during the descent trajectory, with a focus on the re-entry burn, and the resulting heating pattern on the rocket structure. Interesting phenomena which affect the aero-thermodynamic heating of the vehicle surface are represented by the plume spreading, plume-to-plume interactions, immersion of the vehicle in hot exhaust gases and vehicle aerodynamics.

Finally, the numerical model used for CFD computations is validated by comparing the numerical results, obtained for a sub-scale model of the RETALT1, with the wind tunnel experiments performed by the DLR Department of Supersonic and Hypersonic Technologies in Cologne. Such experiments are part of an extensive experimental campaign whose aim is the simulation of the RETALT1 re-entry trajectory. The Hypersonic Wind Tunnel Cologne (H2K) is used for the re-entry burn simulations whereas the aerodynamic phase (without active engines) is studied by means of tests performed in the Trisonic Wind Tunnel Cologne (TMK). Finally, the Vertical Free-jet Facility Cologne (VMK) allows to investigate the exhaust plume occurring during the landing burn with cold gas experiments. An extended version of this paper which includes also additional examples of flow field solutions from CFD analyses can be found on Zenodo platform at the url: `https://doi.org/10.5281/zenodo.6592386`.

2. MATHEMATICAL & NUMERICAL MODEL

The heat flux data at different flight regimes and surface temperatures, used for the aero-thermal data base creation, are provided by an extensive CFD simulations campaign. These CFD analyses are performed with the hybrid structured-unstructured DLR Navier–Stokes solver TAU [8]. The TAU code is a second-order finite-volume flow solver for the Euler and Navier–Stokes equations in their integral forms, using eddy viscosity, Reynolds stress or detached and large eddy simulation for turbulence modelling. The Spalart–Allmaras one-equation eddy viscosity model [9] has been employed for the present investigation. Concerning the numerical scheme, the AUSMDV flux-vector splitting is applied together with MUSCL gradient reconstruction in order to achieve second-order spatial accuracy whilst maintaining a robust numerical treatment of strong discontinuities.

2.1. Thermodynamic model for the RETALT1 flight configuration

The thermodynamic model used for CFD simulations of RETALT1 flight configuration is based on a mixture of thermally perfect gases. The properties of the individual species are either computed from spectroscopic constants using partition functions that include an accurate representation of high temperature effects [10] or from NASA-Polynomials [11]. Appropriate mixture rules are applied to compute the thermodynamic properties depending on the local gas composition, pressure and density. For the computations a chemically frozen mixture of air ($76\,\%\,N_2$ and $24\,\%\,O_2$ by mass fraction) and engine exhaust gas ($97.7\,\%\,H_2O$, $2\,\%\,H_2$, $0.2\,\%\,OH$ and tracer species) is considered. The plume characteristics and exhaust gas composition at the RETALT1 nozzle exit have been obtained by a separate 2D-axisymmetric nozzle simulation where the flow is considered in chemical non-equilibrium and the Jachimowski reaction mechanism, described in Ref. [12], is employed. The resulting flow profiles, as well as the exhaust gas composition, are then prescribed as a Dirichlet inlet condition at the nozzle exit planes in the 3D simulations of the RETALT1 rocket [7].

2.2. Thermodynamic model for the RETALT1 experimental model

The CFD simulations of cold gas experiments on the RETALT1 scaled model are performed considering calorically perfect air as engine fluid. Separated 2D-axisymmetric nozzle simulation are carried out imposing total pressure and total temperature at the nozzle inlet. Also in this case, the resulting flow profiles are then prescribed as a Dirichlet inlet condition at the nozzle exit planes in the actual 3D simulations of the RETALT1 experimental model.

2.3. Structural response model

The aero-thermal database and associated interpolation algorithms provide the aero-thermodynamic heat flux on the rocket surface as function of time, location on the vehicle surface and wall temperature. The coupling of the ATDB to a structural response model allows to evaluate the temperature history during the entire flight path for in each position on the rocket surface.

An simple 0D structural response model is represented by the lumped mass method which describes the instantaneous heating of a chosen material characterized by thickness, δ, density, ρ and heat capacity, c. Starting from a temperature distribution $T\left(x,y,z,t_{old}\right)$, the new temperature distribution $T\left(x,y,z,t_{new}\right)$, evaluated at the time instant $t_{old}+\Delta t$, can be computed as follows:

$$\begin{aligned} T\left(x,y,z,t_{new}\right) &= T\left(x,y,z,t_{old}\right) \\ &\quad + \frac{q_c\left(x,y,z,t_{old}\right) - q_r\left(x,y,z,t_{old}\right)}{\rho c \delta}\Delta t \end{aligned} \tag{1}$$

The temperature evolution is, therefore, driven by the difference of aero-thermodynamic heating, q_c, provided by the ATDB and conveniently interpolated, and the thermal radiation, q_r, divided by the product of the material properties. The thermal radiation is given by Eq.2, where ϵ is the surface emissivity, σ is the Stefan–Boltzmann constant and T_{env} is the environment temperature.

$$q_r\left(x,y,z,t_{old}\right) = \sigma\epsilon\left(T\left(x,y,z,t_{old}\right)^4 - T_{env}^4\right) \tag{2}$$

3. DLR WIND TUNNEL FACILITIES AND RETALT1 EXPERIMENTAL MODEL

The experimental campaign carried out at DLR Department of Supersonic and Hypersonic Technologies in Cologne aims to investigate the RETALT1 re-entry trajectory. The retro-propulsion phase is studied in the Hypersonic Wind Tunnel Cologne (H2K) whereas the aerodynamic phase is tested in the Trisonic Wind Tunnel Cologne (TMK). The landing burn is studied by means experiments performed in the Vertical Free-jet Facility Cologne (VMK).

In this paper representative results of the H2K test series are shown and compared to CFD in order to validate the numerical model. A detail description of the H2K facility is provided in Ref. [13].

Fig. 1: RETALT1 model mounted in H2K facility

The RETALT1 model, mounted in the wind tunnel, is shown in Fig.1. The model has a scaling of 1/130 compared to the RETALT reference configuration, it is equipped with high frequency pressure sensors meant for the detailed analyses of the base flow. For the simulation of the exhaust plume, air was blown out through a hollow model support string and a model Laval nozzle with an expansion ratio of 2.5. Various nozzle segments were manufactured for testing different engine combinations, i.e. one active engine or three active engines with different deflection angles.

4. RETALT1 MISSION AND CFD DATA SETS

This section aims to provide a description of the RETALT1 flight trajectory and the two re-entry scenarios for the RETALT1 first stage recovery. The ascent phase, from the take off until the Main Engine Cut Off (MECO), is attained by exploiting all the 9 LOX/LH2 engines of the first stage. This paper focuses on the analysis of the downrange-landing scenario as this imposes the design driving loads on the rocket configuration.

Right after MECO, the second stage main engine ignites and completes the injection of the payload to orbit. At this point, according to the defined mission, two possible scenarios for the first stage recovery are possible: for Geostationary Transfer Orbit (GTO) missions Down-range Landing (DRL) on a sea platform can be performed while for low earth orbit (LEO) missions, the first stage can accomplish a Return to Launch Site (RTLS), this scenario is not analysed in this paper because DRL imposes the highest heat loads.

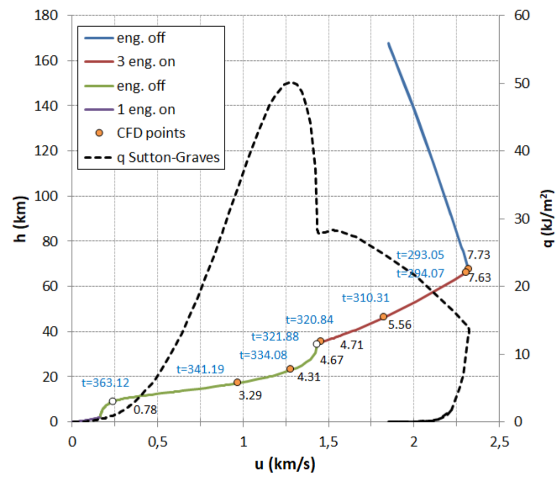

(a) Descent trajectory

#	Time (s)	h (km)	Mach
1	293,048	67,515	7,73
2	294,066	66,178	7,63
3	310,311	46,321	5,561
4	320,838	35,375	4,71
s5	321,857	34,419	4,665
5	334,084	22,962	4,313
6	341,195	17,187	3.291
s6	363.105	8,848	0,777

(b) Database population for descent configuration

Fig. 2: RETALT1 Descent trajectory points and flight conditions

For DRL scenario, the first stage continues the flight along a ballistic trajectory outside of the atmosphere. Before entry, the aerodynamic control surfaces are deployed and the vehicle is turned in a flip over maneuver. After entering the upper atmosphere (blue line in Fig.2a) the re-entry burn, performed with 3 of 9 engines in operation, is initiated to reduce the flight speed (red line). This is followed by an aerodynamic unpropelled flight phase (green line), which is terminated by a landing burn, performed by using only the central engine, in order to ensure a controlled touch down (purple line).

In Fig.2a, the orange symbols indicate trajectory points for which CFD-analyses were performed (# 1-6) instead the white symbols (# s5-s6) indicates synthetic heat flux data computed by scaling the heat flux distribution in points # 5 and # 6 respectively. The scaling is performed by using well established general relationships between the global heat loads and the free stream properties [14, 15], and was only applied for trajectory points during the unpropelled flight phases. The use of a synthetic solution is justified when the fluid-dynamic conditions are not critical for the aero-thermal loads.
The dashed black line provides an estimation of the heat flux in the stagnation point downstream the bow shock and are obtained using the Sutton-Graves empirical equation [14]. Such equation is not able to provide meaningful results in the retro-propulsion regime, due to the presence of the plume.

The free stream conditions in each CFD point for the descent trajectory are summarized in Fig.2b. The CFD computations are performed using fixed wall temperatures of 200K and 600K.

5. CFD REPRESENTATIVE RESULTS

A representative flow field solution for the RETALT1 during the entry trajectory, and in particular at the end of retro-propulsion phase, is shown in Fig.3. The corresponding free stream conditions are described in Tab. 2b: trajectory point # 4. The surface heat flux and the pressure coefficient distribution are shown in color in Fig. 3a and Fig. 3b respectively; gas temperature and Mach number in the symmetry plane are shown in gray-scale. In Fig. 3a, the brown iso-surface depicts the region of the flow field where $u = -100$ m/s in order to visualize the back flow. The streamlines are coloured by the longitudinal velocity component. In Fig. 3b, instead, the brown iso-surface represents the boundary of 50% exhaust mass fraction and indicates the geometrical extend of the engine plumes.

This flow field solution is particularly interesting due to the severe thermal loads occurring on the aerodynamic control surfaces which directly face the incoming flow being heated in the upstream stagnation zone. Due to the moderate densities and the fact that the flow is aligned parallel to the vehicle surface, the heat fluxes on the central body remain moderate. The base plate heating during the retro-burn is not so intense due to the efficient shielding effect of the exhaust plume, see Fig. 3a.
The back flow region is significantly smaller compared to the beginning of retro-propulsion (high altitude mode), here the brown iso-furface is confined in a limited area downstream the launcher and spreads slightly upstream the base plate.

Fig.3b shows that the extent of the exhaust plume is limited and this is due to the increasing static and dynamic free stream pressure that occurs towards the end of the retro-burn. Only the lower part of the launcher is immersed in an atmosphere rich of hot exhausted gases.

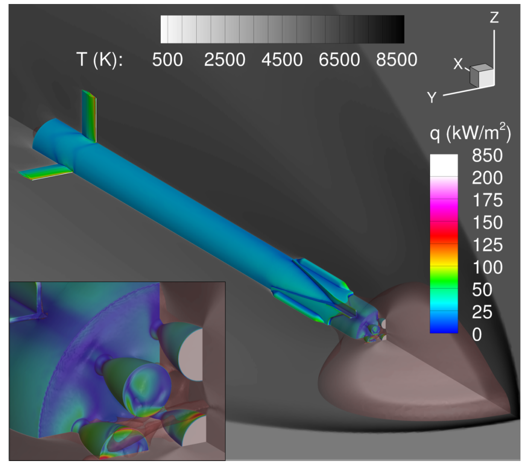

(a) Iso-surface of back flow, temperature, surface heat flux

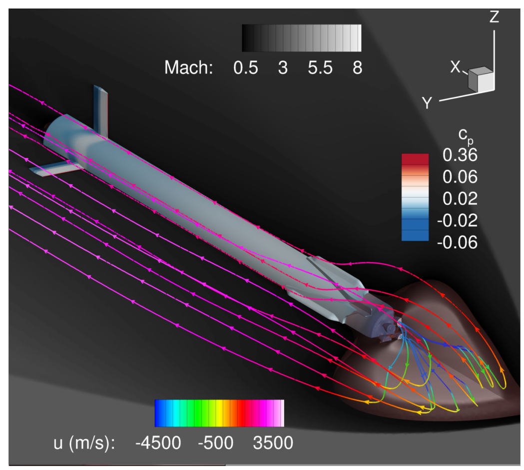

(b) Iso-surface of 50% exhaust mass fraction, Mach number, pressure coefficient

Fig. 3: RETALT1 descent flow field structure (mid-range altitude mode, h=35km, Mach=4.7), end of retro propulsion

5.0.1. Time histories of heat loads

The time history of the average heat fluxes on the base plate and planar fin, during the descent trajectory, are shown in Fig.4. Considering the base plate (Fig.4a), it is possible to observe that the average heat flux remains approximately constant during retro-propulsion because of the exhaust plume shielding effect.

Once the engines are turned off, the average heat flux goes through a sudden increase due to the presence of the bow shock and the associated aero-thermal heating close to the base plate. Between trajectory points #5s-5 the average heat flux slightly decreases, indeed in this part of the trajectory the flow conditions do not change significantly, and then rapidly declines due to the strong reduction of the flight velocity.

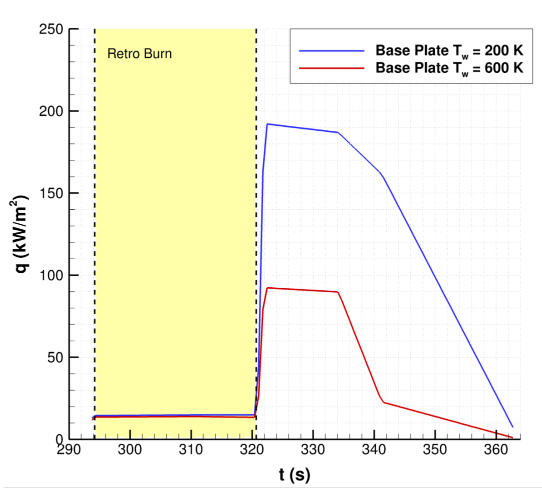

(a) Base plate

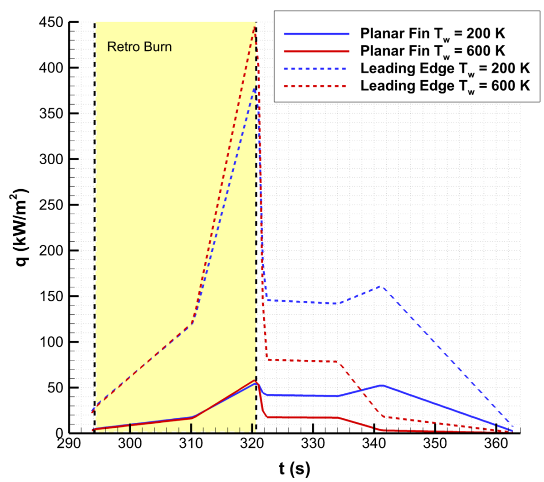

(b) Planar fin and leading edge

Fig. 4: RETALT1 time histories of average heat flux for constant wall temperatures - descent phase

Although the time histories of the averaged heat flux on the overall planar fin and leading edge have the same qualitative trend, the values on the leading edge are much higher ($\approx 86\%$ evaluated at the peak), see Fig.4b. The average heat flux increases for the entire retro-propulsion duration due to the fact that the aerodynamic control surface directly face the incoming flow being heated in the upstream stagnation zone. Such increase of the average heat flux is also due to the larger flow density at lower altitude which leads to more confined plumes. After having reached the maximum value at the end of the retro burn the heat flux drops because the hot exhaust gases are blown away. The curves in Fig.4b exhibit a plateau between trajectory points #5s-5 then they show different trends depending on the wall temperature.

For $T_w = 600$K (red line) the average heat flux decreases because of the strong reduction in flight velocity. Concerning $T_w = 200$K (blue line) the average heat flux starts increasing again and reaches a local maximum. This effect is due to the heating provided by the surrounding atmosphere with the ambient temperature being larger than 200K.

5.0.2. Aero-thermal database application

The temperature history during the RETALT1 flight for each location on the vehicle surface can be computed by coupling the ATDB, together with the interpolation algorithms, to a structural response model as shown in paragraph nr. 2.3. The material properties are summarized in Tab.1.

Table 1: Material properties used for the exemplary lumped-mass thermal analysis

Surface emissivity	ε	0.2	$(-)$
Wall thickness	δ	5	(mm)
Density	ρ	2600	(Kg/m^3)
Heat capacity	c	900	$(J/Kg/K)$

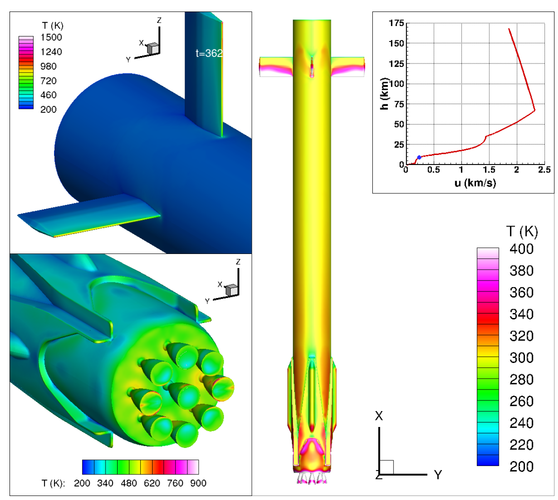

Fig. 5: RETALT1 surface temperature distribution close to the end of return trajectory

Close to the end of the trajectory, the highest temperature occurs on the leading edge of the planar fin, close to the tip, with a peak of 1500K as shown in Fig.5. Concerning the base plate, high temperatures are reached in the area enclosed by the engines cluster especially along Y-axis. During the retro-burn the external surfaces of the not operational engine's nozzles experience peak temperatures of 800K close to the exit plane. The central body, from the the folded legs up to the top, is characterized by an average temperature of 300K, higher values can be found in the bottom part of the launcher.

The time evolution of the average temperature on the planar fin leading edge and on the base plate is shown in Fig.6. About the base plate, it is possible to observe that the rate of increase of the average temperature is rather low during the retro-propulsion phase because of the plume shielding effect. In accordance with Fig.4a, the following sudden temperature increase, during the aerodynamic phase, is due to aerothermal heating provided by the bow shock located close the base plate.

Concerning the planar fin, the average temperature increases with an high rate during the retro-burn due to direct exposure of the control surface to the incoming hot flow. At the end of retro-propulsion, the average temperature keeps increasing but the curve slope decreases significantly. The reason lies in the drop of the total heat flux which essentially corresponds to the aero-thermodynamic heating because of the negligible contribution provided by the thermal radiation. At about t=340 s the temperature starts decreasing because the total heat flux becomes negative. This happens because the aerodynamic control surface is warmer than the surrounding atmosphere and the vehicle Mach number is decreasing.

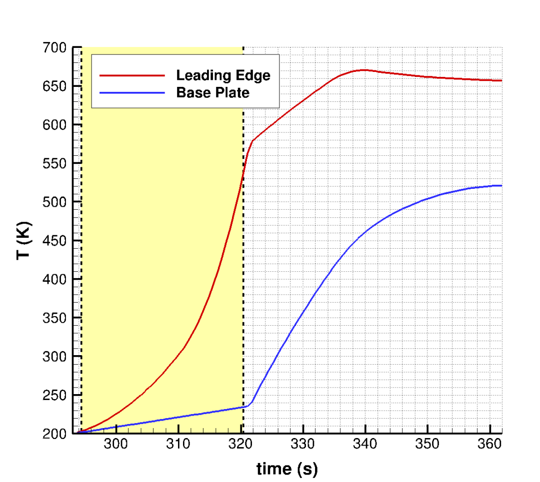

Fig. 6: Time history of the average temperature on the planar fin leading edge and base plate

6. WIND TUNNEL EXPERIMENTS

In this section a comparison between some CFD results and Hypersonic Wind Tunnel Cologne (H2K) tests are compared. H2K facility, in fact, has been used for carrying out an extensive campaign of experiments with the aim to investigate the RETALT1 re-entry burn. A detailed description of the RETALT1 experimental model and configurations can be found in Ref.[5]. The experimental condition are summarized in Tab.2.

Table 2: Experimental test matrix

Comp	Eng	α	Mach	p0 [bar]	T0 [K]	pCC [bar]	TCC [K]
1	0	0	5.29	4	450	0	300
2	1	0	5.29	4	450	20	300
3	1	10	5.29	4	450	20	300
4	3	0	5.29	4	450	12.3	300
4	3	0	5.29	4	450	12.3	300
5	3	10	5.29	4	450	12.3	300
6	3	10	5.29	4	450	12.3	300

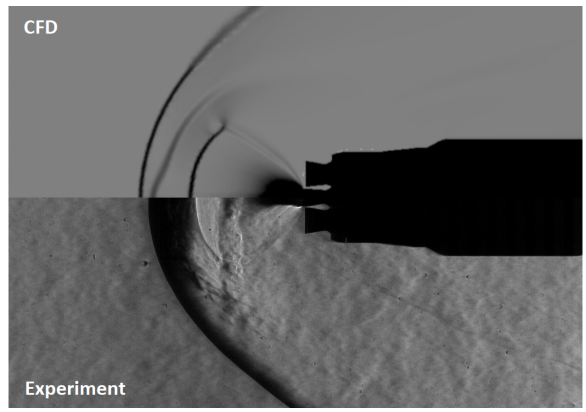

(a) Schlieren pictures comparison: CFD (top) vs. experimental (bottom).

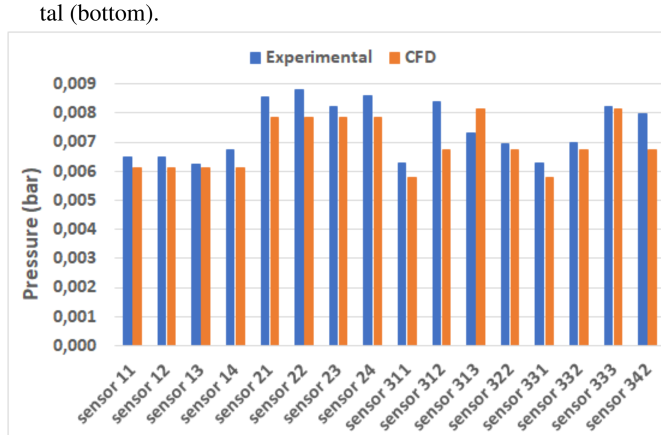

(b) Surface pressure comparison

Fig. 7: Test 2: active central engine, $AoA = 0°$.

Fig.7a shows a comparison between the Schlieren pictures obtained by CFD simulation and wind tunnel measurements for the case with one operative engine (the central one) and angle of attack $AoA = 0°$. The bow shock, in the numerical result, is located slightly farther away from the body than in the experiment and small differences in plume shape can be observed. The flow structure in the plume region is complex due to the incoming hypersonic flow that encounters the jet flow from the engine. Just downstream of the bow shock wave it is possible to observe the mixing region where the free stream air is mixed with the jet coming out of the engine. Since the gases have different densities, the mixing region is characterized by a density gradient. Finally, a Mach disk is formed at the end of the plume. Between the Mach disk and the mixing surface there is a subsonic region.

The pressure, measured by high frequency sensors located on the surface of the RETALT1 experimental model, is then compared to the numerical one. Sensors 11-12-13-14 are placed at beginning of the cylindrical region, 21-22-23-24 are positioned slight upstream the folded legs, 313 and 333 are placed in the region that connects the base plate to the bottom part of the cylindrical body, 312-322-332-342 are on the base plate around the engines cluster and finally 311 and 331 are located close to the central engine. Fig. 7b show that numerical pressure is slightly lower than the experimental one except for sensor 313 where it is higher. The percentage error is below 10% for most of the sensors, instead, for sensors 342 and 312, it takes the values of 18% and 24%, respectively. These data show that there is a very good agreement between the pressure experimentally measured and the pressure computed via CFD despite the extremely complicated flow field which develops close to the base plate due to the plume-plume interactions.

The experiments with 3 operative engines active showed some wavy patterns which indicate the presence of flow unsteadiness. Such unsteady behaviour is remarkable in the case with $AoA = 0°$ whereas is less accentuated when the angle of attack is equal to $10°$. Although the unsteadiness level is lower in the the latter case, a wavy pattern can be noticed downstream the bow shock, see Fig.8a. The presence of an angle of attack different from zero has a stabilizing effect on the flow field and makes the plume asymmetric. Since in the case with $AoA = 10°$ the amplitude of the bow shock oscillations is not so large it is possible to compare a single Schlieren snapshot to the numerical flow field, see Fig.8b.

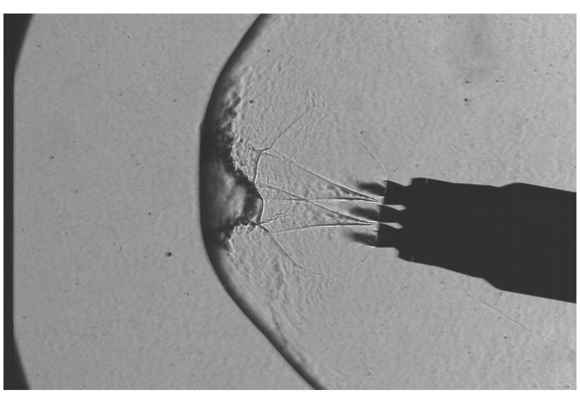

(a) Experimental Schlieren picture

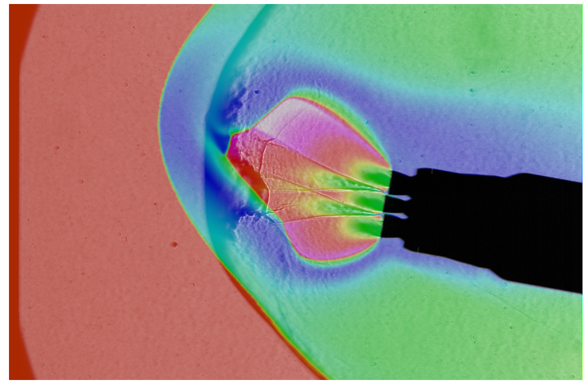

(b) CFD Mach coloured contour superimposed to the experimental Schlieren picture

Fig. 8: Experimental vs. CFD Schlieren, Test 5: 3 operative engines, $AoA = 10°$.

The superposition of the numerical Mach field and the experimental Schlieren picture, represented in Fig.8b, shows that the central structure of the plume is well represented by the CFD simulation instead the Mach disk is more distant from the body compared to the experimental result. Same considerations apply for the bow shock except for the region below the vehicle where a good agreement between the experimental result and the numerical one can be observed.

7. CONCLUSIONS

A fast-response surrogate model for the aero-thermodynamic heating of the RETALT1 launcher, during both the ascent flight and the atmospheric entry, was created. This model is based on an aero-thermal database (ATDB) consisting in a large set of steady-state CFD results for the surface heat fluxes for different flight regimes and surface temperatures. Interpolation algorithms allow the estimation of heat loads as a function of the flight time and local surface temperatures. The computational matrix covered the entire RETALT1 flight trajectory. CFD simulations were performed mainly around peak heating and at critical flight conditions whereas scaling laws are used to evaluate thermal loads in aerodynamic flight conditions characterized by low heating rates. The coupling of the ATDB to a structural response model allows to estimate the temperature history in each location on the vehicle surface during the entire trajectory.

The paper focused on the analysis on the downrange-landing scenario, and in particular on the retro-propulsion phase, since it imposes the design driving loads on the rocket configuration.

A flow field solution and the typical phenomena occurring at the end of retro-burn were analysed. At low altitude, where the static pressure is higher, the exhaust plumes are confined and the intensity of plume-plume interactions on the launcher base plate are less significant. In this phase the flow field conditions provide the most critical thermal load on the leading edge of the planar fin which directly face the incoming flow being heated in the upstream stagnation zone.

The ATDB, along with the interpolation algorithms, was then coupled with a simple structural response model to show the capability of such tool to compute the temperature time evolution on the rocket surface. In particular the time history of the average temperature on the base plate and leading edge of the planar fins was analysed. These components were chosen as representative examples because they experience the most critical thermal loads.

The comparison of CFD calculations with Schlieren pictures from the experiment showed small differences in the bow shock stand-off distance for the case with the central engine active. Larger discrepancies can be observed in the case with 3 operative engines, nevertheless the central structure of the plume is well represented. It is important to highlight that despite the differences between the experimental results and the numerical ones, in terms of the flow field representation, CFD pressure matches very well the measured one for most of the experiments.
In conclusion, the general good agreement between experimental results and CFD computations proves that the selected numerical model and set-up, as well as the meshing criterion, are capable to represent the physical phenomenology of retro propulsion. Such validation justify the use of the same methodology even for the RETALT1 flight configuration.

8. ACKNOWLEDGEMENTS

This project has received funding from the European Union's Horizon 2020 research and innovation framework program under grant agreement No 821890. We gratefully acknowledge the interest in our work and the opportunity to forward this essential research.

9. REFERENCES

[1] A. Marwege, A. Gülhan, J. Klevanski, J. Riehmer, D. Kirchheck, S. Karl, D. Bonetti, J. Vos, M. Jevons, A. Krammer, and J. Carvalho, "Retro propulsion assisted landing technologies (retalt): Current status and outlook of the eu funded project on reusable launch vehicles," *70th International Astronautical Congress (IAC), Washington D.C., United States*, 2019.

[2] S. Paixão, C. Peixoto, M. Reinas, and J. Carvalho, "Retalt tps design and manufacturing," *CEAS Space Journal, https://doi.org/10.1007/s12567-021-00417-w*, 2022.

[3] D. Charbonnier, J. Vos, A. Marwege, and C. Hantz, "Computational fluid dynamics investigations of aerodynamic control surfaces of a vertical landing configurations," *CEAS Space Journal, doi:10.1007/s12567-022-00431-6*, 2022.

[4] A. Marwege, C. Hantz, D. Kirchheck, J. Klevanski, A. Gülhan, D. Charbonnier, and J. Vos, "Wind tunnel experiments of interstage segments used for aerodynamic control of retro-propulsion assisted landing vehicles," *CEAS Space Journal, https://doi.org/10.1007/s12567-022-00425-4*, 2022.

[5] J. Vos, D. Charbonnier, A. Marwege, A. Gülhan, M. Laureti, and S. Karl, "Aerodynamic investigations of a vertical landing launcher configuration by means of computational fluid dynamics and wind tunnel tests," *AIAA SCITECH 2022 Forum, https://doi.org/10.2514/6.2022-1308*, San Diego, 2022.

[6] A. Krammer, L. Blecha, and M. Lichtenberger, "Fin actuation, thrust vector control and landing leg mechanisms design for the retalt vtvl launcher," *CEAS Space Journal, https://doi.org/10.1007/s12567-021-00421-0*, 2022.

[7] M. Laureti and S. Karl, "Aerothermal databases and load predictions for retro propulsion assisted launch vehicles (retalt)," *CEAS Space Journal, https://doi.org/10.1007/s12567-021-00413-0*, 2022.

[8] S. Langer, S. Schwöppe, and N. Kroll, "The dlr flow solver tau—status and recent algorithmic developments," *AIAA Paper 2014-0080*, 2014.

[9] P.R Spalart and S.R Allmaras, "A one-equation turbulence model for aerodynamic flows," *AIAA Paper 1992-0439*, 1992.

[10] B. Bottin, "Aerothermodynamic model of an inductively-coupled plasma wind tunnel," *PhD-Thesis, University of Liege*, 1999.

[11] S. Gordon and B. J. McBride, "Computer program for calculation of complex chemical equilibrium compositions and applications," *NASA Reference Publication 1311*, 1994.

[12] P. Gerlinger, "An implicit multigrid method for turbulent combustion," *Journal of Computational Physics, Vol. 167: 247-276*, 2001.

[13] F.J. Niezgodka, "Der hyperschallwindkanal h2k des dlr in köln-porz (stand 2000)," *DLR-Mitt. 2001-01, Cologne.DOI: 10.13009/ EUCASS2017-680*, 2001.

[14] K. Sutton and R.A. Graves, "A general stagnation point convective heating equation for arbitrary gas mixtures," *NASA TR-R-376*, 1971.

[15] G.T. Chapman, "Theoretical laminar convective heat transfer and boundary layer characteristics on cones at speeds to 24 km/s," *NASA TN D-2463*, 1964.